ACS OMEGA

http://pubs.acs.org/journal/acsodf

Article

Effects of Hydrophobic Modification of Linear- and Branch-Structured Fluorinated and Nonfluorinated Silanes on Mesoporous Silica Particles

Jeong Ho Chang* and Chae Eun Pyo

Cite This: *ACS Omega* 2022, 7, 26661−26669

Read Online

ACCESS | Metrics & More | Article Recommendations | Supporting Information

ABSTRACT: This work reports a comparison of hydrophobic surface modification on mesoporous silica particles (MSPs) obtained by large-scale production using a batch reactor with linear and branched fluorinated and nonfluorinated silanes. Fluorinated silanes were used with TDF-TMOS and TFP-TMOS as a linear and branched structure, respectively. Nonfluorinated silanes were used with OD-TEOS and HMDS as a linear and branched structure, respectively. These four silanes were grafted on the surface of the MSPs as the function of the concentrations, and then, the water contact angles (WCAs) were measured. The WCA of the four silane-grafted MSPs was higher in the branch-structured silanes, namely, TFP-TMOS@MSPs and HMDS@MSPs than in linear-structured silanes, namely, TDF-TMOS and OD-TEOS due to the higher hydrophobicity by a lot of −F and $-CH_3$ groups. Furthermore, the relationship between the WCA and BET parameters was demonstrated using the surface areas, pore volumes, and grafted amounts of the four silane-grafted MSPs. The structural characterization was demonstrated by solid-state ^{29}Si MAS NMR to determine the bonding environment of Si atoms between the grafted silane and the surfaces of MSPs using the T^3/T^2 and Q^3/Q^4 ratios of the fluorinated and nonfluorinated silane-grafted MSPs. Among the four silanes, nonfluorinated HMDS@MSPs had a high contact angle of 135° as fluorinated TFP-TMOS@MSPs. When 5 wt % of HMDS@MSPs mixed with gravure ink was coated on a biodegradable polylactic acid (PLA) film, the contact angle was improved to 131.8 from 83.3° of the natural PLA film.

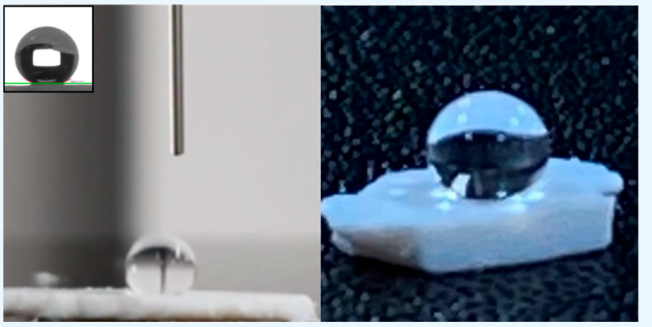

1. INTRODUCTION

Recently, techniques for hydrophobic surface modification have been used in various fields such as self-cleaning, drag reduction, oil−water separation, anticorrosion, antireflective transparent coatings, antifreezing, optical devices, and automobiles through layer-by-layer deposition, cocondensation, lithography, chemical vapor deposition, and sol−gel processes.[1−5] To form a hydrophobic surface, the process of reducing the contact surface between water and the material by using a material with a low surface energy or by increasing the surface roughness has been used.[6−8] The method of lowering surface energy includes increasing the surface roughness through a surface treatment process, such as plasma etching, nanoparticle attachment, chemical vapor deposition, dip coating, and plasma coating.[9−13] A widely used hydrophobic surface modification process involves the use of fluorine compounds, such as polytetrafluoro ethylene (PTFE, Teflon) and perfluoro alkyl groups.[14−16] Because fluorine has a small atomic diameter (42 pm) and a large electronegativity (3.98), it is advantageous for lowering the surface free energy.[17,18] Stable fluorine groups decrease the van der Waals potential with the result that electrostatic interactions limit the contact between the solid and liquid phases, resulting in wider contact angles.[19] In addition, fluorine-based compounds have excellent heat resistance, environmental stability, a low coefficient of friction, and chemical resistance, thereby exhibiting high water-soluble surface properties at about 130 to 160°. For this reason, fluorine-based compounds have been used as a representative of hydrophobic surface modification materials.[20,21] However, the use of fluorine-based compounds is known to cause risks of environmental pollution and incurable diseases (e.g., thyroid disease, cancer, and Alzheimer's syndrome), immune disorders, and human health problems, such as hormonal disorders.[22−24] Furthermore, it is known that about 60−80% of the fluorine-based compounds remains in the skeleton when absorbed into the body and cause inhibition of cholinesterase glycolysis, hemorrhagic gastroenteritis, acute toxic nephritis, and liver damage.[25,26] To overcome these problems, there have been several reports on the use of

Received: May 10, 2022
Accepted: July 12, 2022
Published: July 22, 2022

https://doi.org/10.1021/acsomega.2c02918
ACS Omega 2022, 7, 26661−26669

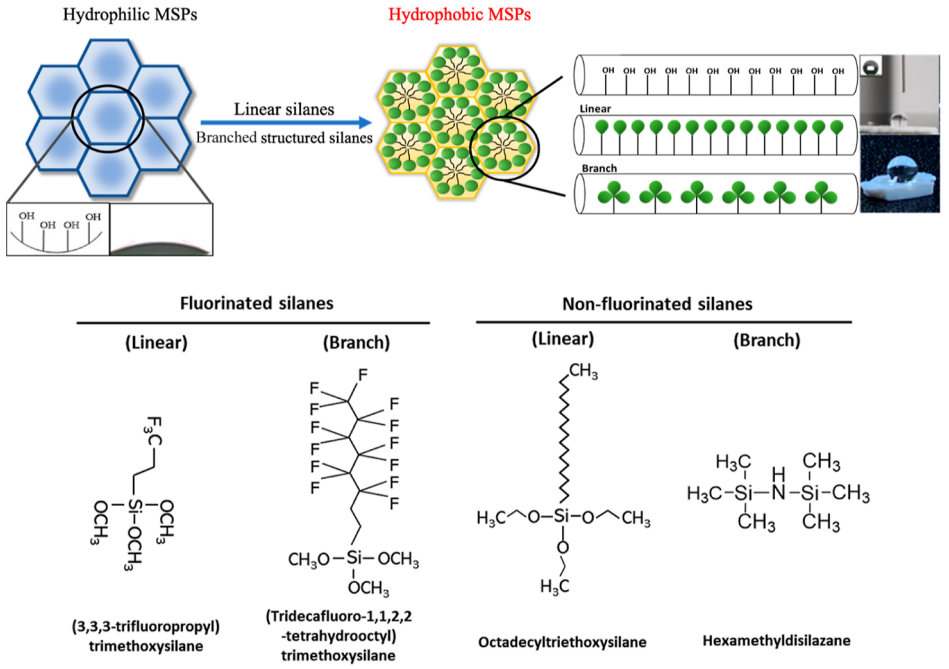

Figure 1. Schemes for the hydrophobic modification and chemical structures of linear- and branch-structured fluorinated and nonfluorinated silanes.

nonfluorinated compounds, such as hydrophobic alkyl chain compounds, for hydrophobic surface modification instead of the use of fluorine-based compounds.[27,28] However, the contact angles of the hydrophobic alkyl chain compounds are not as large as those of the fluorine-based compounds, and there have been no report on changing the contact angle depending on structural factors, such as the length and shape of the alkyl chain of the fluorine and nonfluorine-based compounds.

In this work, we prepared hydrophilic mesoporous silica particles (MSPs) with a high surface area (>800 m^2/g) and many nanopores by large-scale production using a batch reactor, and then we demonstrated surface modification by fluorinated and nonfluorinated silanes, each with two kinds of linear- and branch-structured silanes. Fluorinated silanes, such as 3,3,3-trifluoropropyltrimethoxysilane (TFP-TMOS, linear) and tridecafluoro-1,1,2,2-tetra hydrooctyltrimethoxysilane (TDF-TMOS, branched), and nonfluorinated silanes, such as octadecyltriethoxysilane (OD-TES, linear) and hexamethyldisilazne (HMDS, branch), were used as the linear and branched structures, respectively. In addition, the hydrophobic efficiency was calculated by the function of the concentration (0.4, 0.8, 1.2, and 1.6 M) and the reaction time (24, 48, 72, and 96 h) of linear- and branch-structured fluorinated and nonfluorinated silane-grafted MSPs. Nonfluorinated HMDS@MSPs showed a higher contact angle of 135° as much as fluorinated TFP-TMOS@MSPs. Furthermore, HMDS@MSPs mixed with gravure ink were coated on a biodegradable polylactic acid (PLA) film as a function of the concentration, and their viscosity, turbidity, and contact angle were obtained.

2. EXPERIMENTAL SECTION

2.1. Chemicals and Materials. Pluronic P123 ((poly-(ethyleneoxide)-poly(propyleneoxide)-poly(ethyleneoxide)) was purchased from BASF (Korea). Tetraethyl orthosilicate (TEOS, >99%) and hexamethyl disilazne (99.9%) were purchased from Sigma-Aldrich (Korea). Octadecyl-triethoxysilane (OD-TES), hexamethyldisilazne (HMDS), (3,3,3-trifluoropropyl) trimethoxy silane (TFP-TMOS), and tridecafluoro-1,1,2,2-tetrahydrooctyltrimethoxysilane (TDF-TMOS) were purchased from Gelest (USA). Hexane (95%) was purchased from Daejung Co., Ltd. (Korea).

2.2. Preparation of the MSPs by a Large Scale Process. For the preparation, 13.34 kg of Pluronic P123 was dissolved in 500 L of distilled water by stirring at 45 °C for 24 h, and 14.4 kg of TEOS was added dropwise into a Pluronic P123 solution at 45 °C and stirred for 24 h. The mixture was put in a steel bomb and aged in a vacuum oven at 120 °C for 8 h. The powder was filtered, washed with ethanol and distilled water, and dried at room temperature. Calcination was achieved by 6 h at 550 °C.

2.3. Fluorinated Silane and Nonfluorinated Silane Modification on MSPs as a Function of the Concentration. Fluorinated silanes, namely TFP-TMOS and TDF-TMOS, and nonfluorinated silanes, namely OD-TES and HMDS were used as the linear and branched structures. Then, 1.0 g of MSPs was stirred in 24 mL of hexane for 2 h and then added to each concentration of fluorinated or nonfluorinated silanes (0.4, 0.8, 1.2, and 1.6 M). The mixture was refluxed at 70 °C for 24 h. Finally, the solution was filtered and washed with ethanol and dried at room temperature.

2.4. HMDS Modification on MSPs and the HMDS@MSPs-Gravure Ink Solution. HMDS modification on MSPs (HMDS@MSPs) as a function of the reaction time was demonstrated, and 1.0 g of MSPs was stirred in 24 mL of hexane for 2 h, and then 1.6 M HMDS was added to this solution. The mixture was kept for 4 days and then filtered, washed with ethanol, and then dried at room temperature.

Moreover, each amount of HMDS@MSPs (0, 0.1, 0.3, 0.5, and 0.7 g) was added to 10 mL of gravure ink solution and then stirred for 24 h. After dropping 100 μL of this solution on a biodegradable PLA film, it was dried for 24 h.

https://doi.org/10.1021/acsomega.2c02918
ACS Omega 2022, 7, 26661−26669

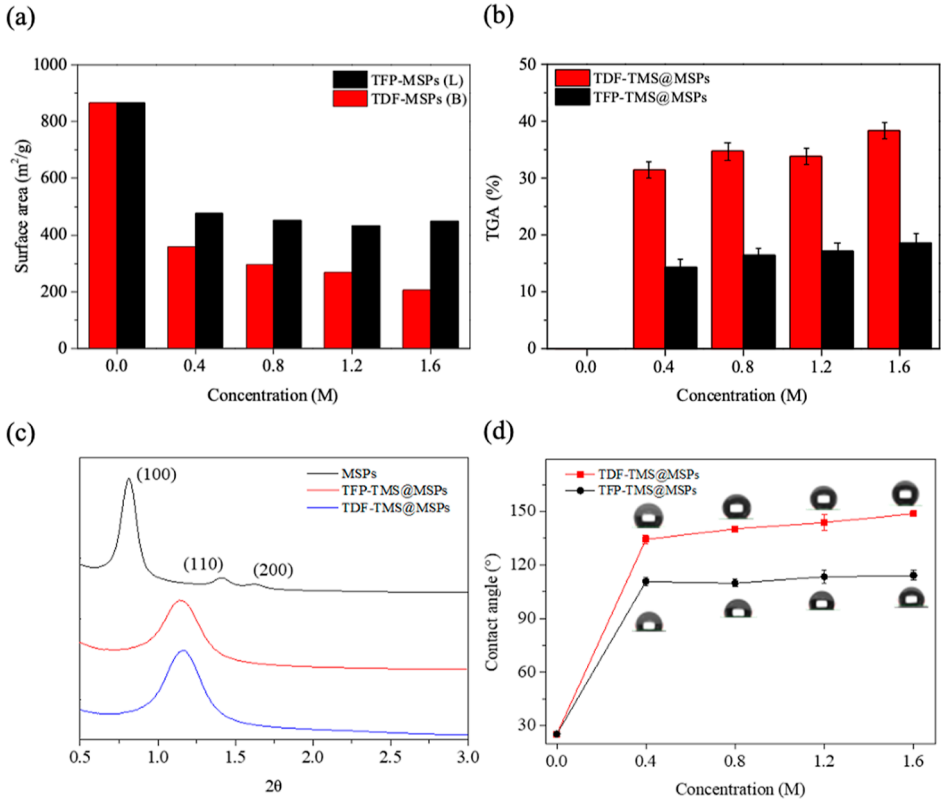

Figure 2. (a) BET surface areas and (b) TGA analysis of fluorinated silanes, such as TFP-TMS @MSPs and TDF-TMS @MSPs, (c) small angle XRD of MSPs, TFP-TMS @MSPs and TDF-TMS @MSPs, and (d) WCAs of TFP-TMS @MSPs and TDF-TMS @MSPs as a function of the concentration.

2.5. Instrumentation Analysis. The contact angle measurement was confirmed by water contact angle (WCA) analysis using a contact angle analyzer from Git Soft Tech. The WCA was measured three times with 10 μL of distilled water, and then a digital camera captured a picture of it. The Brunauer–Emmett–Teller (BET) analyses were performed with the ASAP 2420. Identification and characterization of the alkyl-silane-modified MSPs were carried out using thermogravimetric analysis (TGA) and solid-state ^{29}Si magic angle spinning nuclear magnetic resonance (MAS NMR). TGA was performed with a Q600 TA instrument at a rate of 10 °C min^{-1} in an N_2 gas from 25 °C to 700 °C. The solid-state ^{29}Si-MAS NMR measurements were performed in a 9.4 T Bruker Ascend 400WB instrument using a 4 mm zirconia rotor with a pulse length of 1.6 μs, spinning rate of 11 kHz, and a repetition delay of 20 s. The morphological and structural details of the MSPs were studied by field emission scanning electron microscopy (FE-SEM) and transmission electron microscopy (TEM). FE-SEM investigations were carried out with a Tescan Mira-3 instrument using 2 kV of accelerating voltage. TEM was carried out on a JEOL JEM-2100 electron microscope operated at 200 kV. Small angle and wide-angle X-ray diffraction (XRD) were performed using SmartLab and Miniflex 600 (Rigaku) with scan ranges of 1.5–5 and 10–90°, respectively.

3. RESULTS AND DISCUSSION

3.1. Preparation and Characterization of MSPs. The prepared MSPs were obtained from highly ordered nanopores and channels using a batch reactor with large-scale production, as shown in the Supporting Information (Figure S1). The characterization of the MSPs was demonstrated by TEM, nitrogen adsorption and desorption isotherm by BET, and WCAs, as previously reported.[29] The TEM image showed the hexagonally ordered porous structure and straight channels with 7.44 nm, and the N_2 adsorption–desorption isotherms showed an H4 type hysteresis loop with a specific surface area of 753.16 m^2/g, and the average contact angle was 25.44°, respectively (Figure S2).

Figure 1 shows the scheme for hydrophobic modification on mesoporous silica surfaces with linear- and branch-structured silanes and their chemical structures. The linear-structured silanes were used with TFP-TMS and ODTES, and the branch-structured silanes were used with TDF-TMS and HMDS, corresponding to fluorinated and nonfluorinated silanes, respectively.

3.2. Hydrophobic Properties of the Fluorinated-Silane- Modified MSPs as a Function of the Silane Concentration. Figure 2a shows the BET surface areas of fluorinated TFP-TMS@MSPs and TDF-TMS@MSPs as a function of the silane concentration. As the silane concentration increased, the surface areas of the TFP-TMS@MSPs and TDF-TMS@MSPs decreased. The MSPs had a surface area of 865.96 m^2/g, but the TDF-TMS@MSPs had surface areas of 357.25, 295.77, 266.92, and 204.52 m^2/g, corresponding to 0.4, 0.8, 1.2, and 1.6 M, respectively, while, the TFT-TMS@MSPs had surface areas of 476.7, 452.98, 432.69, and 449.03 m^2/g, corresponding to 0.4, 0.8, 1.2, and 1.6 M, respectively. Comparing the specific surface areas of TFP-TMS@MSPs and TDF-TMS@MSPs, TDF-TMS@MSPs had a smaller surface area than the TFP-TMS@MSPs. The specific surface areas were reduced due to interaction with the –OH

https://doi.org/10.1021/acsomega.2c02918
ACS Omega 2022, 7, 26661–26669

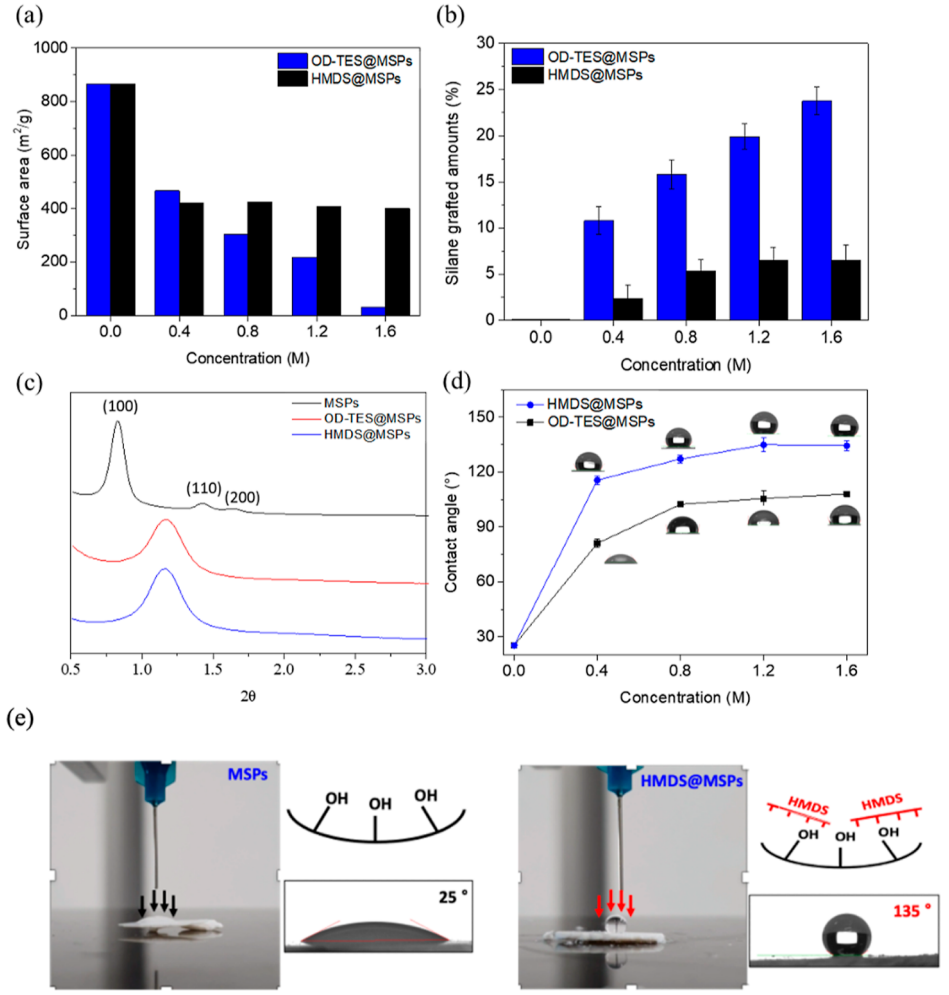

Figure 3. (a) BET surface areas and (b) TGA analysis of nonfluorinated silanes, such as OD-TES@MSPs and HMDS@MSPs, (c) small angle XRD of MSPs, OD-TES@MSPs, and HMDS@MSPs, (d) WCAs of OD-TES@MSPs and HMDS@MSPs as a function of the concentration, and (e) comparison of WCAs of MSPs and HMDS@MSPs.

group on the MSP surface because TDF-TMS has a relatively larger molecular size and weight than that of TFP-TMS@MSPs. Figure 2b shows the TGA analysis for TFP-TMS@MSPs and TDF-TMS@MSPs and reveals the differences in grafted amounts between TFP-TMS and TDF-TMS as a function of the silane concentration. The grafted amounts of TDF-TMS on MSPs as a function of the silane concentration were 31.44, 34.73, 33.87, and 38.36%, respectively. Also, the grafted amounts of TFP-TMS on MSPs as a function of the silane concentration were 14.29, 16.40, 17.16, and 18.60%, respectively. The TGA results confirmed that TDF-TMS, which had a larger molecule size and molecular weight, was more grafted to the surface of the MSPs than TFP-TMS. Furthermore, Figure 2c shows the small-angle XRD patterns of the MSPs, TFP-TMS@MSPs and TDF-TMS@MSPs. The characteristic diffractions of MSP (100), (110), and (200) are seen at 0.817, 1.413, and 1.630 of 2 θ, respectively. As grafted fluorinated silanes on the MSPs, the characteristic diffraction of (100) of TFP-TMS@MSPs and TDF-TMS@MSPs was shifted to 1.150 and 1.170 from 0.187 of MSPs due to the pore confinement by the modification. Moreover, no diffractions of (110) and (200) of TMS@MSPs and TDF-TMS@MSPs were observed. Figure 2d shows the WCAs of TFP-TMS@MSPs and TDF-TMS@MSPs as a function of the silane concentration. The contact angles of TDF-TMS@MSPs as a function of the silane concentration were 134.26°, 140.16°, 143.75°, and 148.6°, corresponding to 0.4, 0.8, 1.2, and 1.6 M, respectively. On the other hand, the contact angles of TFP-TMS@MSPs were 110.63, 109.74, 113.35, and 114.15°, corresponding to 0.4 M, 0.8 M, 1.2 M, and 1.6 M, respectively. The contact angles of branch-structured TDF-TMS@MSPs were higher than that of linear TFP-TMS@MSPs. This was because the grafting efficiency on MSPs of TDF-TMS is higher than that of TFP-TMS, which is confirmed by BET and TGA analysis that TDF-TMS@MSPs had lower surface areas and higher grafted amounts, as shown in Figure 2a,b. Moreover, the pore volumes of the TDF-TMS@MSPs decreased from 1.25 cm^3/g of MSPs to 0.28, 0.24, 0.22, and 0.17 cm^3/g corresponding to 0.4, 0.8, 1.2, and 1.6 M of the TDF-TMS concentration.

On the other hand, the pore volumes of the TFP-TMS@MSPs decreased to 0.44, 0.37, 0.37, and 0.35 cm^3/g, corresponding to 0.4, 0.8, 1.2, and 1.6 M of the TFP-TMS concentration. Moreover, the nitrogen adsorption−desorption isotherms of TFP-TMS@MSPs and TDF-TMS@MSPs were obtained as a function of the silane concentration, and their isotherms showed a collapse of the hysteresis loop in the relative pressure (P/P_0) of 0.42−0.65 with an increased TDF-

https://doi.org/10.1021/acsomega.2c02918
ACS Omega 2022, 7, 26661−26669

TMS and TFP-TMS concentration. This means that the pore size significantly narrows as the silane concentration of TDF-TMS and TFP-TMS to be grafted on the surface of the mesoporous silica increases, as shown in the Supporting Information (Figure S3).

3.3. Nonfluorinated Silane Modification on MSPs as a Function of the Concentration. Figure 3a shows the BET surface areas of nonfluorinated OD-TES@MSPs and HMDS@MSPs as a function of the silane concentration. The change in the surface areas of the OD-TES@MSPs as a function of the silane concentration decreased remarkably from 865.96 m^2/g of MSPs to 466.09, 304.53, 217.52, and 31.1 m^2/g, corresponding to 0.4, 0.8, 1.2, and 1.6 M of OD-TES, respectively. However, the change in the surface areas of the HMDS@MSPs did not decrease much as a function of the silane concentration, which were 420.35, 424.45, 408.02, and 400.56 m^2/g, corresponding to 0.4, 0.8, 1.2, and 1.6 M of HMDS, respectively. These results are also consistent with TGA analysis, as shown in Figure 3b. The grafted amounts of the OD-TES in OD-TES@MSPs as a function of the concentration increased remarkably to 10.79, 15.79, 19.91, and 23.78%, but HMDS increased slightly as 2.32, 5.3, 6.48, and 6.52%, corresponding to 0.4, 0.8, 1.2, and 1.6 M of OD-TES and HMDS, respectively. Furthermore, Figure 3c shows the small-angle XRD patterns of MSPs, OD-TES@MSPs, and HMDS@MSPs. The characteristic diffractions of MSPs, namely (100), (110), and (200), are seen at 0.817, 1.431, and 1.640 of 2 θ, respectively. As nonfluorinated silanes were grafted on the MSPs, the characteristic diffraction of (100) of OD-TES@MSPs and HMDS@MSPs was shifted to 1.163 from 1.167 of 2 θ due to the pore confinement by the modification. Moreover, no diffractions of (110) and (200) of OD-TES@MSPs and HMDS@MSPs were not observed. Figure 3d shows the contact angles of MSPs, OD-TES@MSPs, and HMDS@MSPs as a function of the silane concentration. The contact angles of linear OD-TES@MSPs and branch-structured HMDS@MSPs as a function of the silane concentration were 81.08, 102.35, 105.60, 108.05, and 115.66, 127.2, 135, and 135°, corresponding to 0.4, 0.8, 1.2, and 1.6 M of OD-TES and HMDS, respectively. The contact angles of branch-structured HMDS@MSPs were higher than those of linear OD-TES@MSPs. This was due to the structural confirmation effect of HMDS. Although the small-sized HMDS was not much grafted on MSPs and showed a higher surface area, as shown in Figure 3a,b, HMDS easily blocked the hydroxyl groups (−OH) on the surface of MSPs due to the short distance between $-CH_3$ of HMDS and −OH of MSPs in the grafting reaction. The OD-TES was sparsely grafted on the surface of MSPs due to the bulky structure. Furthermore, HMDS surface modification on MSPs improved the hydrophobic contact angle of MSPs from 25.44 to 135°, which is 5.3 times higher than that of MSPs, as shown in Figure 3e. Moreover, the nitrogen adsorption−desorption isotherms of OD-TES@MSPs and HMDS@MSPs were obtained as a function of the silane concentration, and their isotherms showed a typical type IV and the distinct hysteresis loop of H2 in the relative pressure (P/P_0) of 0.42−1.0, with an increased OD-TES and HMDS concentration, as shown in the Supporting Information (Figure S3).

3.4. Solid-State ^{29}Si MAS NMR of the Fluorinated and Nonfluorinated MSPs. ^{29}Si-MAS NMR spectroscopy has been extensively used to determine the bonding environment of Si atoms near the surfaces in a mesoporous silica matrix.[30,31] Figure 4 shows the ^{29}Si-MAS NMR spectra of fluorinated- and nonfluorinated-silane-modified MSPs comparing the MSPs.

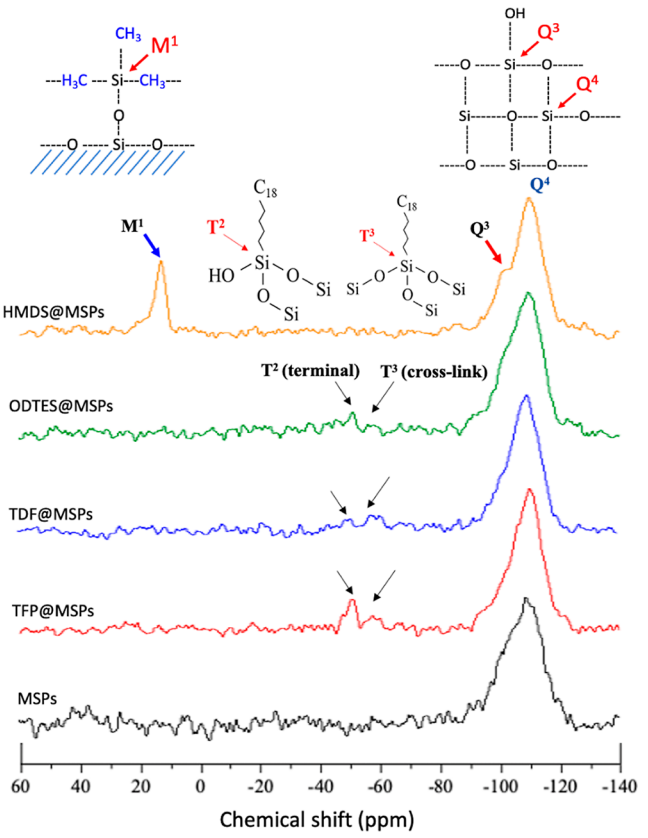

Figure 4. Solid-state ^{29}Si MAS NMR of the fluorinated and nonfluorinated MSPs.

We note that the intensities in the spectra allow qualitative estimation of the relative populations of the different M^n, T^n, and Q^n sites.[32] All samples show a strong chemical shift at −90 to −130 ppm, corresponding to Q^3 (Si-(**OSi**)$_3$OR) and Q^4(Si-(OSi)$_4$), respectively. Moreover, TFP-TMS@MSPs, TDF-TMS@MSPs, and OT-TES@MSPs show a chemical shift at −50 to −70 ppm, corresponding to T^2 (R−**Si**(OSi)$_2$(OH), terminal siloxane) and T^3(R−**Si**(OSi)$_3$, cross-linking), respectively. Since HMDS@MSPs do not have silanol groups, the T^n and Q^n sites do not appear, and only a chemical shift at 10 to 20 ppm, corresponding to M^1 (R_3-**Si**-R′) is shown. In the silane modification on the silica support, the Q^3 Si sites play a crucial role since they provide the Si−OH groups for silane modification, and Q^4 Si sites do not directly participate in the modification process as they lack OH groups. The T^3/T^2 ratios were 0.59, 2.69, and 2.92, corresponding to TFP-TMS@MSPs, TDF-TMS@MSPs, and OT-TES@MSPs. The Q^3/Q^4 ratios were 0.31, 0.38, 0.41, and 0.48 corresponding to TFP-TMS@MSPs, TDF-TMS@MSPs, OT-TES@MSPs, and HMDS @MSPs, respectively. This means that both fluorinated and nonfluorinated branch-structured silanes were strongly grafted on the MSP surface rather than the linear-structured silanes.

3.5. Comparison of Contact Angles of the Fluorinated and Nonfluorinated MSPs. Figure 5a shows a comparison of contact angles with linear- and branch-structured fluorinated and nonfluorinated MSPs. The contact angles are higher in branch-structured silane-modified MSPs, namely TDF-TMS@MSPs and HMDS@MSPs, than in linear-

https://doi.org/10.1021/acsomega.2c02918
ACS Omega 2022, 7, 26661−26669

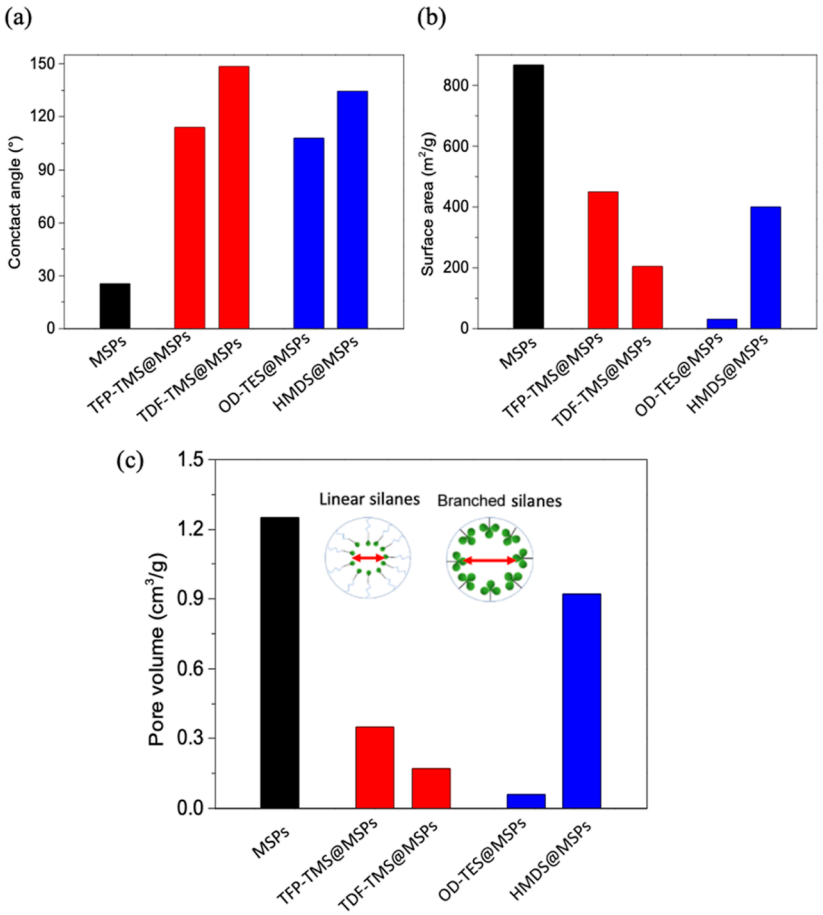

Figure 5. Comparison of (a) contact angles, (b) surface areas, and (c) pore volumes of linear- and branch-structured fluorinated and nonfluorinated MSPs.

structured silane-modified MSPs, namely TFP-TMS@MSPs and OD-TES@MSPs.

In the fluorinated MSPs, the branch-structured TDF-TMS@MSPs with 13 fluorine groups have higher contact angles than the linear TFP-TMS@MSPs with 3 fluorine groups. Furthermore, in the nonfluorinated MSPs, the branch-structured HMDS@MSPs have higher contact angles than the linear OD-TES@MSPs with 3 fluorine groups due to the many hydrophobic methyl ($-CH_3$) groups. HMDS@MSPs have the six hydrophobic methyl ($-CH_3$) groups as a branch structure and are grafted near the MSP surface to screen the hydrophilic $-OH$ groups of the MSP surface effectively. However, OD-TES@MSPs have a hydrophobic methyl ($-CH_3$) group at the terminal of the linear alkyl chains ($-CH_2$) and do not effectively screen the hydrophilic $-OH$ groups due to the structural rotation and bend of alkyl single bonds in spite of the higher grafted amounts on the surface of MSPs (confirmed by TGA analysis). Figure 5b shows a comparison of the N_2 adsorption−desorption isotherms of linear- and branch-structured fluorinated and nonfluorinated MSPs. With these silanes grafted on MSPs, the surface areas were decreased, and the hysteresis loops were changed to an H4 type hysteresis loop from an H2 type. When the fluorinated silanes were grafted on MSPs, the quantity of N_2 adsorption and desorption of the branch-structured TDF-TMS@MSPs was lower than that of the linear-structured TFP-TMS@MSPs due to the lower surface areas. Moreover, the linear-structured OD-TES@MSPs had a much lower quantity of N_2 adsorption and desorption due to the lower pore volumes. However, the HMDS@MSPs had an H3-type hysteresis loop and a higher quantity of N_2 adsorption and desorption. Figure 5c shows a comparison of the pore volume with linear- and branch-structured fluorinated and nonfluorinated MSPs, respectively. The pore volumes are 1.25, 0.22, 0.37, 0.26, and 0.94 cm^3/g, corresponding to MSPs, TFP-TMS@MSPs, TDF-TMS@MSPs, OD-TES@MSPs, and HMDS@MSPs, respectively. The change in the pore volume was decreased in the grafted linear-structured silanes MSPs rather than in the grafted branch-structured silanes due to the longer single alkyl chain length. The HMDS@MSPs had a higher pore volume due to their short alkyl-chained structure.

To compare the relationship between the contact angle of HMDS@MSPs and the reaction time, the modification of the MSPs was observed for 4 days. Figure 6 shows the correlation of the contact angle, surface area, and thermogravimetric analysis results of HMDS @MSPs as a function of the reaction time. As the reaction time increased, the contact angle of the HMDS@MSPs slightly increased to 134.94°, 135.02°, 135.41°, and 135.46°, corresponding to 1, 2, 3, and 4 days, respectively. In spite of the increase in the reaction time used for HMDS modification of the MSPs, the surface areas of the HMDS@MSPs were similar (373.39 to 408.02 m^2/g). The graft amounts and the pore volumes (not shown) of the HMDS@MSPs were in the range of 6.48 to 6.81% and 0.90 to 0.94 cm^3/g, respectively.

https://doi.org/10.1021/acsomega.2c02918
ACS Omega 2022, 7, 26661−26669

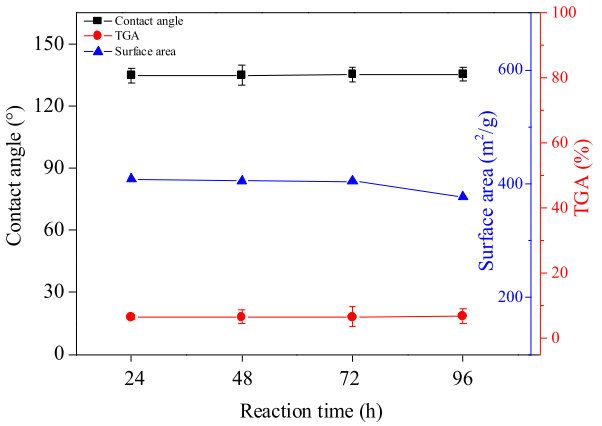

Figure 6. Correlation of the contact angle, surface area, and thermogravimetric analysis results of HMDS@MSPs as a function of the reaction time.

3.6. Gravure Printing Application with HMDS@MSPs on a Biodegradable PLA Film. Gravure printing is widely used in many industrial fields because it is a fast, roll-to-roll print process capable of a high volume.[33,34] The gravure printing system is composed of two cylinders such as an engraved roll and a backing roll. When the gravure roll comes into contact with a plastic or film substrate that is fed between the two rolls, the ink is transferred to the substrates. Gravure ink is made of organic solvents such as methyl ethyl ketone (MEK) and ethyl acetate (EA). For application to gravure printing with HMDS@MSPs, we evaluated the change in contact angles after a mixture of the HMDS@MSPs in gravure ink in amounts of 1, 3, 5, and 7 wt % was dripped onto the biodegradable PLA film, as shown in Figure 7a. The reason that the amount of HMDS@MSPs added to gravure ink is limited to 7% is that the viscosity becomes too high for printing at higher concentrations. Figure 7a shows the pictures of the droplets of only gravure ink and 5% HMDS@MSPs mixture on PLA films before and after addition of water. After the water droplets were sprayed onto the film, the droplets in the gravure solution spread as if they were dispersed over the film, but in the 5% HMDS@MSPs mixture, the droplets appeared to have formed separately. Moreover, the figure shows the contact angles of the HMDS@MSPs mixture in the gravure solution as a function of the amounts, and they increased to 97.89, 114.13, 131.84, and 134.76°, corresponding to 1, 3, 5, and 7% of the HMDS@MSPs mixture from 83.3° of only gravure ink. When the amount of the HMDS@MSPs mixture in the gravure solution was more than 5%, the viscosity was too high to be used as a gravure printing ink. Figure 7b shows the viscosity changes as a function of the amounts of the HMDS@MSP mixture in the gravure solution. Furthermore, we evaluated the relation between the contact angles and the number of droplet layers of the HMDS@MSPs mixture in the gravure solution on the PLA film. The contact angles were not changed by the number of droplet layers of the HMDS@MSPs mixture in the gravure solution, and the contact angles were

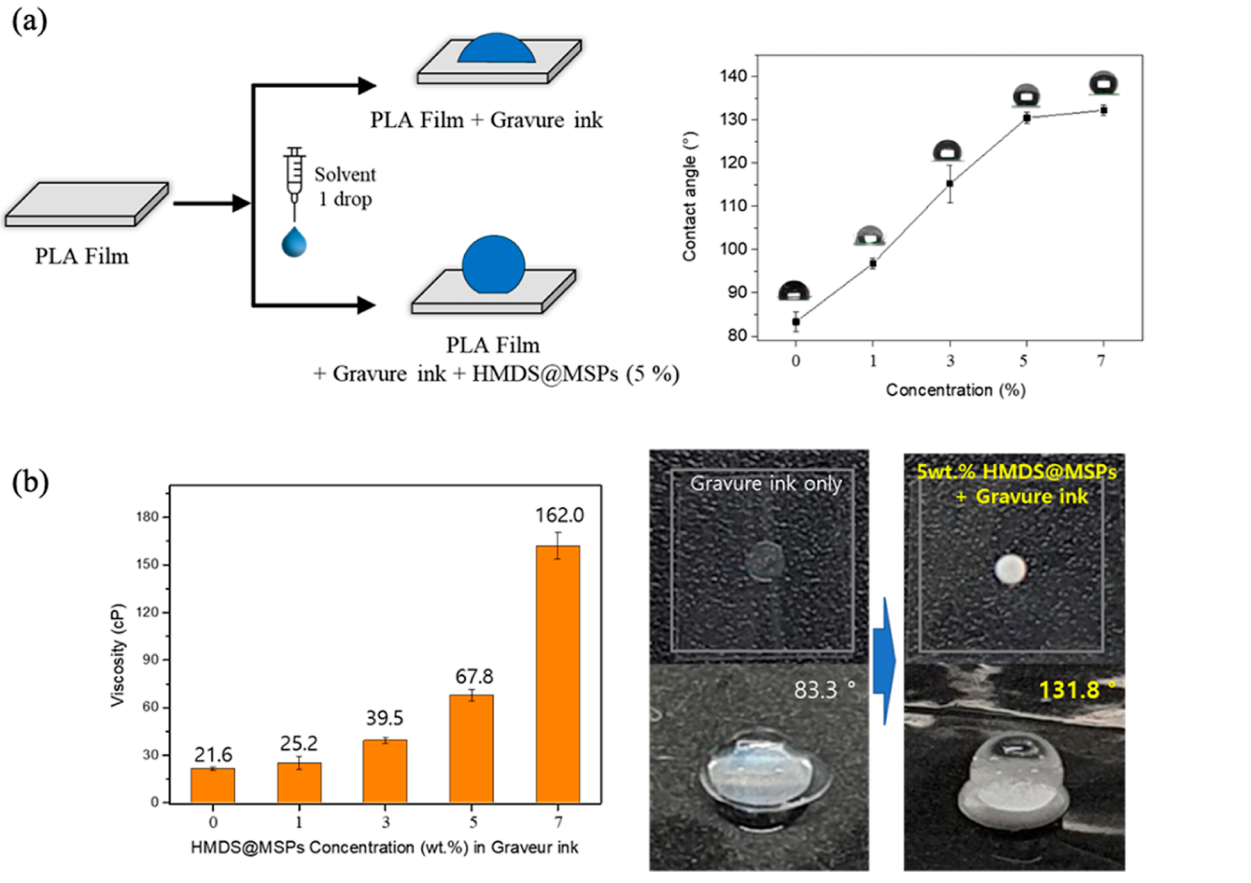

Figure 7. (a) Gravure printing with HMDS@MSPs on a biodegradable PLA film as a function of the concentration, and (b) viscosity changes as a function of the amounts of the HMDS@MSPs mixture in a gravure solution, and the images of a droplet of HMDS@MSPs in the gravure solution on a PLA film.

https://doi.org/10.1021/acsomega.2c02918
ACS Omega 2022, 7, 26661−26669

higher at a higher concentration of the HMDS@MSPs mixture in the gravure solution.

4. CONCLUSIONS

The mesoporous silica was prepared by the sol−gel method and modified to a hydrophobic surface using fluorinated and nonfluorinated silanes as a function of the structure, namely linear (TDF-TMOS, OD-TES) and branched (TFP-TMS, HMDS). The WCAs were higher in branch-structured silanes, namely TFP-TMOS and HMDS, than in linear-structured silanes, namely TDF-TMOS and OD-TEOS, for both fluorinated and nonfluorinated silanes. The WCA values of the four silane-grafted MSPs were related to their surface areas, pore volumes, and the amounts of grafted silanes after the silanes were modified. Structural characterization was achieved by solid-state ^{29}Si NMR to determine the bonding environment of Si atoms near the surfaces and showed the branch-structured silanes of both fluorinated and nonfluorinated were strongly grafted on the MSP surface but not on the linear-structured silanes. Finally, we evaluated the change in contact angles after a mixture of the HMDS@MSPs in gravure ink was dripped onto the biodegradable PLA film. The WCA of 5 wt % of HMDS@MSPs on PLA was enhanced to 131.84 from 83.3° of the natural PLA film.

■ ASSOCIATED CONTENT

Supporting Information

The Supporting Information is available free of charge at https://pubs.acs.org/doi/10.1021/acsomega.2c02918.

Schemes of large-scale production of MSPs; TEM images, small-angle XRD pattern, and BET isotherm of MSPs; nitrogen adsorption−desorption isotherms of linear- and branch-structured fluorinated and non-fluorinated silanes as a function of the silane concentration (PDF)

■ AUTHOR INFORMATION

Corresponding Author

Jeong Ho Chang − *Korea Institute of Ceramic Engineering and Technology, Jinju, Gyeongnam 52851, Korea;* Present Address: Present address: Center for Convergence Bioceramic Materials, Korea Institute of Ceramic Engineering and Technology, Chungbuk 28160, Korea; orcid.org/0000-0002-8222-4176; Email: jhchang@kicet.re.kr

Author

Chae Eun Pyo − *Korea Institute of Ceramic Engineering and Technology, Jinju, Gyeongnam 52851, Korea*

Complete contact information is available at: https://pubs.acs.org/10.1021/acsomega.2c02918

Notes

The authors declare no competing financial interest.

■ ACKNOWLEDGMENTS

This work was supported by a grant from the R&D program funded by the Ministry of Trade, Industry, and Energy (MOTIE, Korea), part of the Industry Core Technology Development Program funded by the Korea Evaluation Institute of Industrial Technology (KEIT) [20003970].

■ REFERENCES

(1) Zeng, Y.; Fan, J.; Chen, S.; He, S.; Yi, Z.; Ye, X.; Yi, Y. Preparation of composite micro/nano structure on the silicon surface by reactive ion etching: Enhanced anti-reflective and hydrophobic properties. *Superlattices Microstruct.* **2018**, *117*, 144−154.

(2) Wang, F.; Li, S.; Wang, W. Fabrication of artificial super-hydrophobic lotus-leaf-like bamboo surfaces through soft lithography. *Colloids Surf., A* **2017**, *513*, 389−395.

(3) Qi, Y.; Yang, Z.; Chen, T.; Xi, Y.; Zhang, J. Fabrication of superhydrophobic surface with desirable anti-icing performance based on micro/nano-structures and organosilane groups. *Appl. Surf. Sci.* **2020**, *501*, 144165.

(4) Bouvet-Marchand, A.; Graillot, A.; Abel, M.; Koudia, M.; Boutevin, G.; Loubat, C.; Grosso, D. Distribution of fluoroalkylsilanes in hydrophobic hybrid sol−gel coatings obtained by co-condensation. *J. Mater. Chem. A* **2018**, *6*, 24899−24910.

(5) Brown, P. S.; Bhushan, B. Bioinspired, roughness-induced, water and oil super-philic and super-phobic coatings prepared by adaptable layer-by-layer technique. *Sci. Rep.* **2015**, *5*, 14030.

(6) Boo, C.; Lee, J.; Elimelech, M. Engineering surface energy and nanostructure of microporous films for expanded membrane distillation applications. *Environ. Sci. Technol.* **2018**, *50*, 8112−8119.

(7) Wang, J.; Wu, Y.; Cao, Y.; Li, G.; Liao, Y. Influence of surface roughness on contact angle hysteresis and spreading work. *Colloid Polym. Sci* **2020**, *298*, 1107−1112.

(8) Söz, C. K.; Yilgör, E.; Yilgör, I. Influence of the average surface roughness on the formation of superhydrophobic polymer surfaces through spin-coating with hydrophobic fumed silica. *Polymers* **2015**, *62*, 118−128.

(9) Jeyasubramanian, K.; Hikku, G. S.; Preethi, A. V. M.; Benitha, V. S.; Selvakumar, N. Fabrication of water repellent cotton fabric by coating nano particle impregnated hydrophobic additives and its characterization. *J. Ind. Eng. Chem.* **2016**, *37*, 180−189.

(10) Guo, X.-J.; Xue, C.-H.; Sathasivam, S.; Page, K.; He, G.; Guo, J.; Promdet, P.; Heale, F. L.; Carmalt, C. J.; Parkin, I. P. Fabrication of robust superhydrophobic surfaces via aerosol-assisted CVD and thermo-triggered healing of superhydrophobicity by recovery of roughness structures. *J. Mater. Chem. A* **2019**, *7*, 17604−17612.

(11) Gurav, A. B.; Xu, Q.; Latthe, S. S.; Vhatkar, R. S.; Liu, S.; Yoon, H.; Yoon, S. S. Superhydrophobic coatings prepared from methyl-modified silica particles using simple dip-coating method. *Ceram. Int.* **2015**, *41*, 3017−3023.

(12) Cho, S. W.; Kim, J. H.; Lee, H. M.; Chae, H.; Kim, C. K. Superhydrophobic Si surfaces having microscale rod structures prepared in a plasma etching system. *Surf. Coat. Technol.* **2016**, *306*, 82−86.

(13) Xu, P.; Coyle, T. W.; Pershin, L.; Mostaghimi, J. Super-hydrophobic ceramic coating: Fabrication by solution precursor plasma spray and investigation of wetting behavior. *J. Colloid Interface Sci.* **2018**, *523*, 35−44.

(14) Liang, Y.; Ju, J.; Deng, N.; Zhou, X.; Yan, J.; Kang, W.; Cheng, B. Super-hydrophobic self-cleaning bead-like SiO_2@ PTFE nanofiber membranes for waterproof-breathable applications. *Appl. Surf. Sci.* **2018**, *442*, 54−64.

(15) Scarratt, L. R.; Hoatson, B. S.; Wood, E. S.; Hawkett, B. S.; Neto, C. Durable superhydrophobic surfaces via spontaneous wrinkling of teflon AF. *ACS Appl. Mater. Interfaces* **2016**, *8*, 6743−6750.

(16) Yuan, N.; Gong, X. R.; Han, B. H. Hydrophobic fluorous metal−organic framework nanoadsorbent for removal of hazardous wastes from water. *ACS Appl. Nano Mater.* **2021**, *4*, 1576−1585.

(17) Li, N.; Zeng, F.; Wang, Y.; Qu, D.; Hu, W.; Luan, Y.; Dong, S.; Zhang, J.; Bai, Y. Fluorinated polyurethane based on liquid fluorine elastomer (LFH) synthesis via two-step method: the critical value of thermal resistance and mechanical properties. *RSC Adv.* **2017**, *7*, 30970−30978.

(18) Thiehoff, C.; Rey, Y. P.; Gilmour, R. The fluorine gauche effect: a brief history. *Isr. J. Chem.* **2017**, *57*, 92−100.

(19) Xing, L.; Keefer, C.; Brown, M. F. Fluorine multipolar interaction: Toward elucidating its energetics in binding recognition. *J. Fluorine Chem.* **2017**, *198*, 47−53.
(20) Cardinaud, C. Fluorine-based plasmas: main features and application in micro-and nanotechnology and in surface treatment. *C. R. Chim.* **2018**, *21*, 723−739.
(21) Pedna, A.; Pinho, L.; Frediani, P.; Mosquera, M. J. Obtaining SiO2−fluorinated PLA bionanocomposites with application as reversible and highly-hydrophobic coatings of buildings. *Prog. Org. Coat.* **2016**, *90*, 91−100.
(22) Zuo, H.; Chen, L.; Kong, M.; Qiu, L.; Lü, P.; Wu, P.; Yang, Y.; Chen, K. Toxic effects of fluoride on organisms. *Life Sci.* **2018**, *198*, 18−24.
(23) Han, J.; Kiss, L.; Mei, H.; Remete, A. M.; Ponikvar-Svet, M.; Sedgwick, D. M.; Roman, R.; Fustero, S.; Moriwaki, H.; Soloshonok, V. A. Chemical aspects of human and environmental overload with fluorine. *Chem. Rev.* **2021**, *121*, 4678−4742.
(24) Fuge, R. Fluorine in the environment, a review of its sources and geochemistry. *Appl. Geochem.* **2019**, *100*, 393−406.
(25) Kyzer, J. L.; Martens, M. Metabolism and toxicity of fluorine compounds. *Chem. Res. Toxicol.* **2021**, *34*, 678−680.
(26) Sharma, D.; Singh, A.; Verma, K.; Paliwal, S.; Sharma, S.; Dwivedi, J. Fluoride: a review of pre-clinical and clinical studies. *Environ. Toxicol. Pharmacol.* **2017**, *56*, 297−313.
(27) Vazirinasab, E.; Momen, G.; Jafari, R. A non-fluorinated mechanochemically robust volumetric superhydrophobic nanocomposite. *J. Mater. Sci. Technol.* **2021**, *66*, 213−225.
(28) Zhao, X.; Khandoker, M. A. R.; Golovin, K. Non-fluorinated omniphobic paper with ultralow contact angle hysteresis. *ACS Appl. Mater. Interfaces* **2020**, *12*, 15748−15756.
(29) Pyo, C. E.; Chang, J. E. Hydrophobic mesoporous silica particles modified with nonfluorinated alkyl silanes. *ACS Omega* **2021**, *6*, 16100−16109.
(30) Seo, H.; Choi, I.; Whiting, N.; Hu, J.; Luu, Q. S.; Pudakalakatti, S.; McCowan, C.; Kim, Y.; Zacharias, N.; Lee, S.; Bhattacharya, P.; Lee, Y. Hyperpolarized porous silicon nanoparticles: potential theragnostic material for ^{29}Si magnetic resonance imaging. *ChemPhysChem* **2018**, *19*, 2143−2147.
(31) Kumari, B.; Brodrecht, M.; Breitzke, H.; Werner, M.; Grünberg, B.; Limbach, H. H.; Forg, S.; Sanjon, E. P.; Drossel, B.; Gutmann, T.; Buntkowsky, G. Mixtures of alcohols and water confined in mesoporous silica: A combined solid-state NMR and molecular dynamics simulation study. *J. Phys. Chem. C* **2018**, *122*, 19540−19550.
(32) Issa, A. A.; Luyt, A. S. Kinetics of alkoxysilanes and organoalkoxysilanes polymerization: A Review. *Polymers* **2019**, *11*, 537−577.
(33) Herzog, N.; Brilmayer, R.; Stanzel, M.; Kalyta, A.; Spiehl, D.; Dörsam, E.; Hess, C.; Andrieu-Brunsen, A. Gravure printing for mesoporous film preparation. *RSC Adv.* **2019**, *9*, 23570−23578.
(34) Park, J.; Nguyen, H. A. D.; Park, S.; Lee, J.; Kim, B.; Lee, D. Roll-to-roll gravure printed silver patterns to guarantee printability and functionality for mass production. *Curr. Appl. Phys.* **2015**, *15*, 367−376.

https://doi.org/10.1021/acsomega.2c02918
ACS Omega 2022, 7, 26661−26669